Proceedings World Geothermal Congress 2020+1
Reykjavik, Iceland, April - October 2021

Development of Powder Metallurgy Based Metal Matrix Composites for Geothermal Applications

Sandeep Irukuvarghula[1], Raja Khan[1], Nick Ludford[1], Frazer Brownlie[2,3], Alastair Pearson[2], Trevor Hodgkiess[2,4], Alessandro Sergi[5,6], Malallah Al Lawati[5,6], Moataz Attallah[5]

[1]TWI Ltd, Cambridge, United Kingdom

[2]Weir Group PLC (The), Glasgow, United Kingdom

[3]Department of Mechanical and Aerospace, University of Strathclyde, Glasgow
[4]Porthan Ltd, Lochgilphead

[5]School of Metallurgy and Materials, University of Birmingham

[6]National Structural Integrity Research Centre (NSIRC), Cambridge

Sandeep.irukuvarghula@twi.co.uk

Keywords: Powder Metallurgy, Hot Isostatic Pressing, Metal Matrix composites, Geothermal, Erosion, Corrosion

ABSTRACT

Materials used in geothermal environment, depending on their location within the power plant, are subjected to several degradation mechanisms such as corrosion due to dissolved CO_2, H_2S, NH_3 gases, sulphate and chloride ions, and erosion from the suspended solids in the geothermal fluid. Erosion-corrosion/erosion-wear is a major degradation mechanism for titanium based materials that are traditionally used to manufacture pumps for geothermal power plants. Metal Matrix Composites (MMCs) are a class of materials that can potentially have better erosion corrosion and wear properties compared to the traditional metallic alloys, and therefore, are of particular interest. In this study, we report our findings on the development of INCONEL625 (IN625) and Ti-6Al-4V (Ti64) base MMCs manufactured using powder metallurgy hot isostatic pressing (PM HIP). Ceramic powders with 10 vol.% of silicon carbide (SiC) and titanium diboride (TiB_2) in IN625 and Ti64 powders, respectively, were blended and consolidated via PM HIP process. In-situ reactions occurred between the metal and ceramic phases in the MMC powders during consolidation, which resulted in the bulk specimens containing complex microstructures. It was found that the hardness of IN625 and Ti64 base MMCs more than doubled compared with HIPed IN625 and Ti64 alloys whilst the erosion-corrosion rate almost halved. Room temperature Charpy impact tests revealed that the mode of fracture was ductile, although a reduction in the ductility of the HIPed MMCs was observed.

1. INTRODUCTION

Geothermal power plants operate at high temperature and pressure conditions, and geothermal sources being aggressive natural environments, pose severe challenges to the structural integrity of various components such as well casings, well heads, turbines, pumps, valves, heat exchangers etc. For the materials used in these applications, common materials degradation mechanisms include corrosion due to dissolved CO_2, H_2S, NH_3 gases and sulphate and chloride ions, erosion from the suspended solids or precipitates in the geothermal fluid that is circulated at high flow rates, and scale formation consisting of silica, sulphides and calcite. Higher enthalpy fluids, which increase the output of geothermal systems, could be accessed by drilling deeper wells (Karlsdottir, 2012). However, geothermal fluids become more aggressive as we go deeper, which in-turn increases the rate at which materials degradation mechanisms proceed (e.g. corrosion rate, erosion rate), and affect the component and plant efficiency. Therefore, in order to address these challenges, GeoCoat project is aimed towards development of (a) coatings on existing materials and (b) new materials using advanced manufacturing techniques that can withstand harsh geothermal conditions.

One of the work packages within the EU funded GeoCoat project involves the development of powder metallurgy (PM) base metal matrix composites (MMCs) for pump application. MMCs contain a controlled volume fraction of a ceramic phase in a ductile metal matrix, and therefore have a combination of the attributes of metals (high ductility) and ceramics (low density and high wear resistance) (Kainer, 2006). PM HIP is a solid state powder consolidation process wherein the principal parameters that control densification and microstructural evolution are temperature, pressure and dwell time (Wilkinson and Ashby, 1975; Helle et al, 1985; Li et al, 1993; Kaysser et al, 1988, Atkinson and Davies, 2000). In PM HIP, densification of a powder compact is principally via athermal plastic yielding, and to a lesser extent, via power law creep and diffusional processes. The yield strength of most materials is strain rate sensitive, and decreases considerably at high homologous temperatures and very low strain rates (i.e. the rate of deformation). Since the strain rates encountered during HIP are very low ($<< 10\text{-}4\ s^{-1}$), HIP parameters are chosen depending on the high temperature strength of the corresponding bulk material at very slow stain rates.

Because of the inter-diffusion of chemical elements in pre-blended powders (i.e. between those present in ceramic and metallic powders) during high temperature consolidation, interaction layers with varying microstructure and chemistry will develop at the interface of ceramic and metallic regions. Additional thermodynamically stable brittle phases, potentially detrimental to the mechanical properties, could possibly be formed during the consolidation process. While the nucleation of a particular phase is dictated by thermodynamics, its growth is controlled by kinetics, which is dependent on the powder consolidation conditions. Since the volume fraction of these phases is a function of the initial volume fraction of ceramic particles and powder consolidation conditions, it is therefore important to optimise the initial volume fraction of ceramic particles and the consolidation process parameters. In this work, mixtures/blended metal and ceramic powders were consolidated via PM HIP process. The main objective

of the present work was to consolidate two type MMC powders, ie IN625+10vol.%SiC and Ti64+10vol.%TiB_2 using PM HIP and evaluate their microstructure, mechanical and tribological properties.

2. MATERIALS AND METHODS

Powders that were used for the production of MMCs were procured from two different sources. Specifically, argon gas atomised (AGA) IN625 and Ti64 powders (i.e. metal powders) with 15-45µm size range were sourced from Carpenter Additive previously known as LPW Technology Ltd, UK while alpha SiC (99.5% purity with <5µm average particle size) and TiB_2 (99.7% purity with <10µm average particle size) powders (i.e. ceramic powders) were procured from Reade Advanced Materials, USA. Powder particle size distribution (PSD) and surface morphology were obtained as per ASTM B822-10 and ASTM E3-11, respectively. The metal and ceramic powders (Table 1) were uniformly mixed using a Speedmixer™ DAC 150.1 FVZ-K system for the production of MMC materials by PM HIP process using EPSI HIP equipment, which has the capability of achieving a maximum temperature and a maximum argon pressure of 1450°C and 200MPa, respectively. This system has a working vessel chamber size of Ø150mm with 300mm height. A schematic of PM HIP production route is shown in Figure 1. Pre-blended powders were packed in specially designed cylindrical shaped sacrificial mild steel canisters with ~2mm wall thickness up to their packing density during the HIP trials. A canister size of Ø50mm and 170mm height was used for the HIP trials. The powder filling operation was performed by placing the partially filled canisters on a shaking platform with intermittent powder filling until the canister was filled up to its full packing density. The shaking platform ensures effective filling of the canisters with each shaking cycle lasting for about ten minutes. However, this technique will not be suitable for pre-blended powders with very distinct density, particle sizes and shapes, as it may disturb the initial homogeneous distribution of reinforcement particles. Therefore, MMC powders were filled in the canisters with few intermediate 'taps' while the shaking platform was only used for filling the canisters with metal powders (IN625 and Ti64 alloys) without any reinforcement particles.

Table 1 Compositions of IN625 and Ti64 base MMCs and the processing conditions for HIP trials

HIP run no.	Composition (Vol.%)	Isostatic pressure (MPa)	Temperature (°C)	Dwell time (min)
1	IN625	120	1160	180
2	IN625+10%SiC	120	1160	180
3	Ti64	140	950	360
4	Ti64+10%TiB_2	140	1160	180

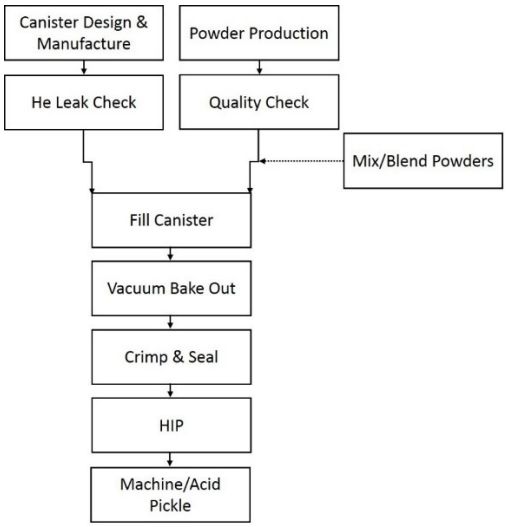

Figure 1 Schematic of PM HIP production route

The powder filled canisters were degassed at warm temperature (<100°C) to achieve a vacuum level better than 10^{-3} mbar. The degassing dwell time was 24 hours as small air pockets and moisture trapped inside the powder travel slowly from the bottom to the top of the powder filled canister, after which the powder filling/evacuating tubes on the canisters were hot crimped and sealed using an oxy-acetylene torch and a crimping device. Manufacturing of the canisters is one of the most critical steps in PM HIP as any defects present in the initial powder filled canister will lead to a failure in consolidating the powder to its theoretical density. The HIP conditions used for the metal and MMC powders are shown in Table 1.

The microstructures of hot isostatically pressed (HIPed) materials were characterised using light optical and scanning electron microscopes while hardness, toughness, and erosion-corrosion performance were evaluated using Vicker microhardness, Charpy

impact and WARC erosion-corrosion test rig (Figure 2), respectively. Secondary electron and backscattered electron images were obtained using Zeiss Sigma Field Emission Gun Scanning Electron Microscope (FEG-SEM) at 25kV, although lower voltages were also used to obtain images with higher resolution. For microscopy, the MMC specimens were ground and polished up to ¼ micron using standard metallographic procedures. Final polishing using Struers OP-U solution was performed for 10 minutes to obtain scratch free surfaces. A qualitative chemical compositional analysis of different microstructural features (phases) was performed using Energy-dispersive X-ray (EDX) system attached to the SEM equipment. Vickers microhardness data were collected at 10 different locations with a load of 0.5kg. Erosion-corrosion tests were performed on Ø38mm x 3mm size HIPed specimens by Weir using a submerged impinging slurry jet apparatus as described previously (Brownlie, 2018) (Figure 2), with the testing conditions as per Table 2. Room temperature Charpy impact tests were performed on 10mm x 10mm x 55mm size HIPed samples with a 2mm Charpy V notch as per BS EN ISO148-2:2016 standard. The instrument had 450 Joules nominal striking energy and three tests per specimen composition were performed. Secondary electron images of the impact tested specimen surfaces were obtained in order to understand the fracture mechanisms in MMCs.

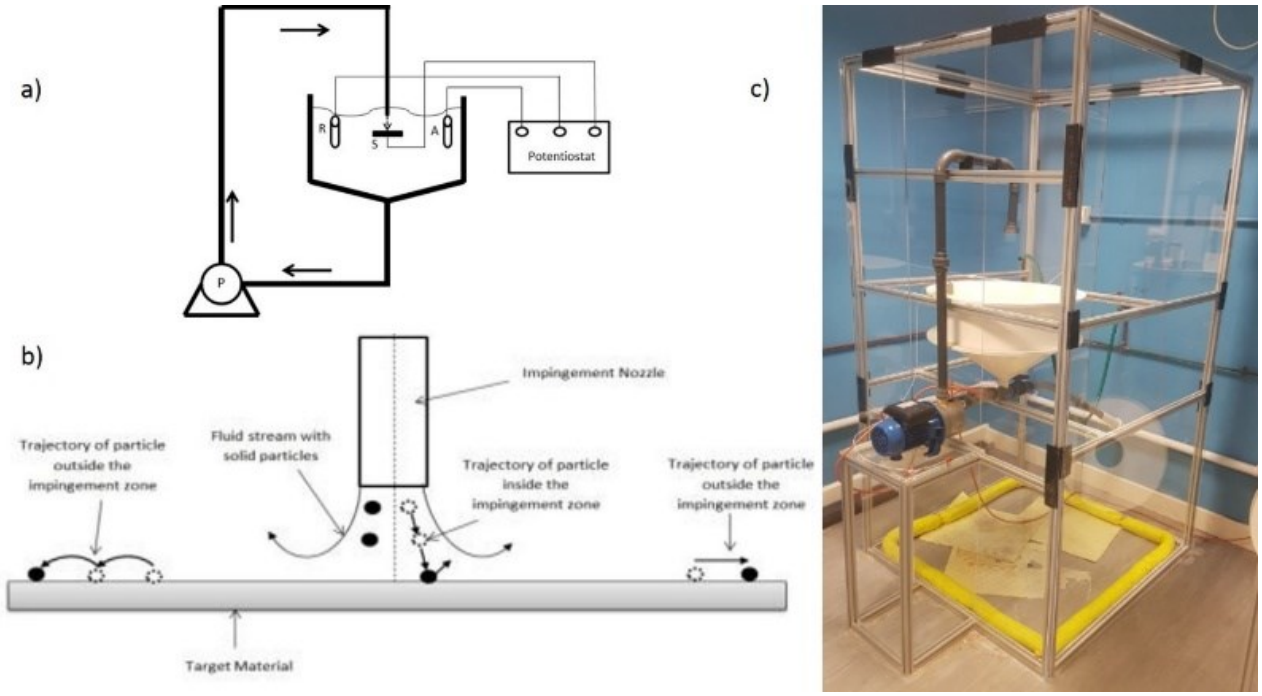

Figure 2 Erosion-corrosion testing; a) schematic of recirculating slurry jet impingement rig with electrochemical monitoring system, b) schematic of slurry jet impingement on the testing material and c) WARC erosion-corrosion test rig at WEIR

Table 2 Erosion-corrosion test conditions

Environment	Free erosion-corrosion (FEC) & cathodic protection (CP)
Temperature	40±1°C
Nozzle diameter (mm)	4
Flow velocity (m/s)	18
Sand concentration (g/l)	0.68
Test duration (mins)	60
Sand type	400µm angular silica
Offset distance between nozzle and test specimen (mm)	5
Impingement angle	90°
NaCl concentration (%)	3.5
pH	4

3 RESULTS

Figure 3 shows PSD of the as-received powders. IN625 powder showed a uni-modal size distribution and D_{50} was measured to be 32µm (Figure 3a). Similar to IN625 powder, the size distribution of Ti64 powder was uni-modal as well, with D50 value of 33µm (Figure 3b). The PSD data for TiB_2 powder (Figure 3c) showed that majority of the particles are between 1µm to 10µm, with very little fraction extending up to 0.3µm whereas D_{50} was measured to be 5.0µm. The PSD for SiC powder (Figure 3d) showed that most of the particles were between 1µm – 10µm with a small fraction of sub-micron size particles (seen as a small hump on the left side of the main peak) and some powders apparently between 20 to 200µm (a hump on the right side of the main peak) whereas D50 was measured to be 4.6µm. PSDs of the two powder mixtures, i.e., IN625+10%SiC and Ti64+10%TiB_2 are shown in Figure 4a and Figure 4b, respectively. As expected, a bimodal distribution was measured, with each peak corresponding to the metal and ceramic phase, respectively. Surface morphology of the as-received powders is shown in Figure 5. AGA IN625 powder was generally spherical, although non-spherical powders can also be seen (Figure 5a). Almost all powders possess satellites (small particles adhering to large particles). Figure 5b shows surface morphology of AGA Ti64 powder. Compared to AGA IN625 powder, AGA Ti64 powder was generally more spherical, although few non-spherical powders can also be seen. A less amount of satellites were observed in AGA Ti64 powder while compared with AGA IN625 powder (Figure 5b). Figure 5c and Figure 5d showed powder morphology of TiB_2 and SiC powder, respectively. Particles are irregularly shaped with facets type particles which is typical for the powders manufacturing via mechanical comminution (crushing and milling). TiB_2 are slightly larger than SiC, which is also reflected in the value of D_{50} (Figure 3c and 3d).

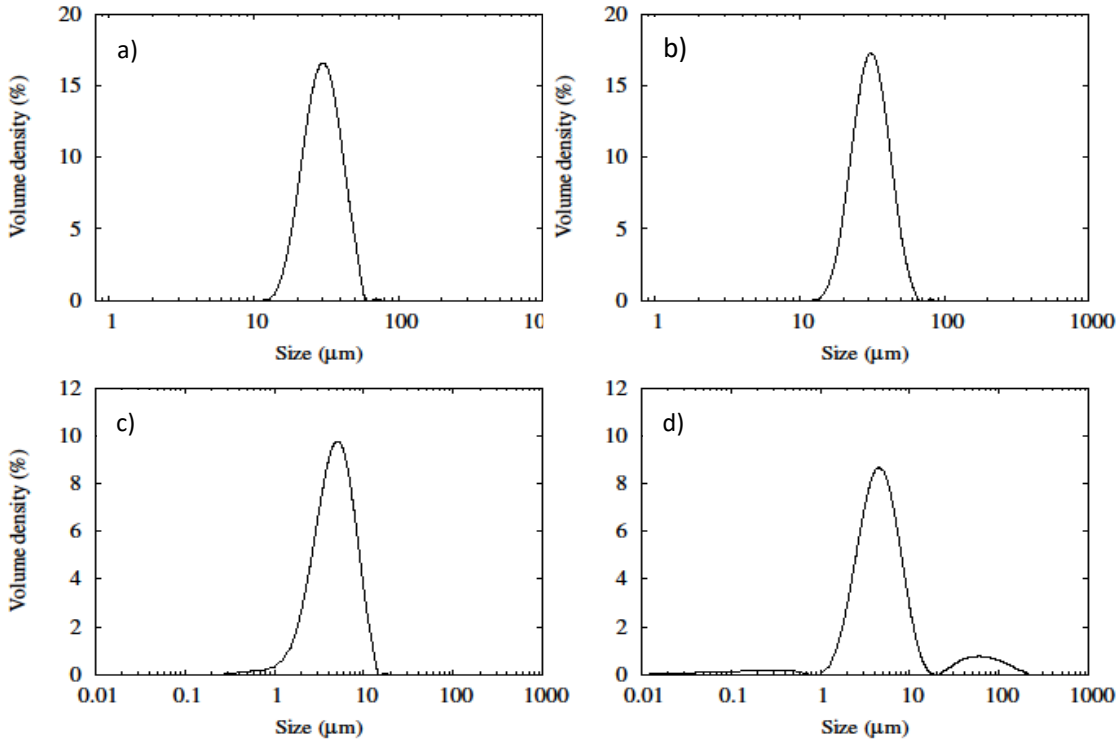

Figure 3 PSD of as-received powders (a) IN625 (b) Ti64 (c) TiB_2 and (d) SiC

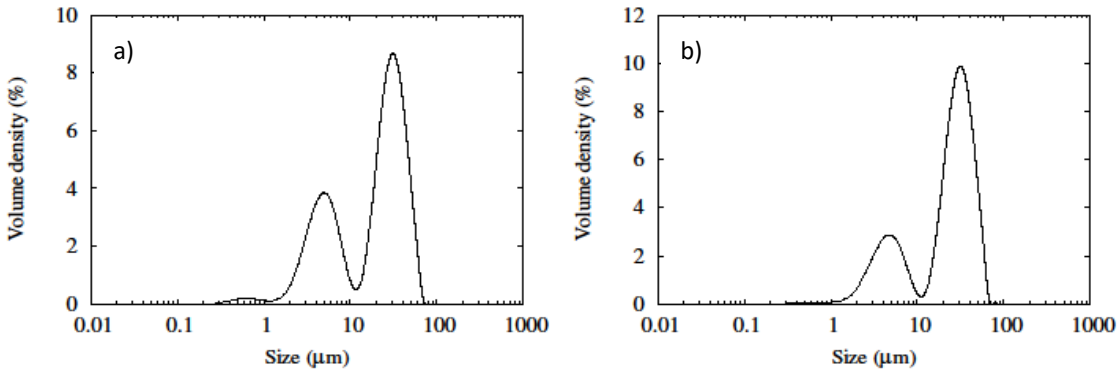

Figure 4 PSD of blended powders (a) IN625+10%SiC (b) Ti64+10%TiB_2

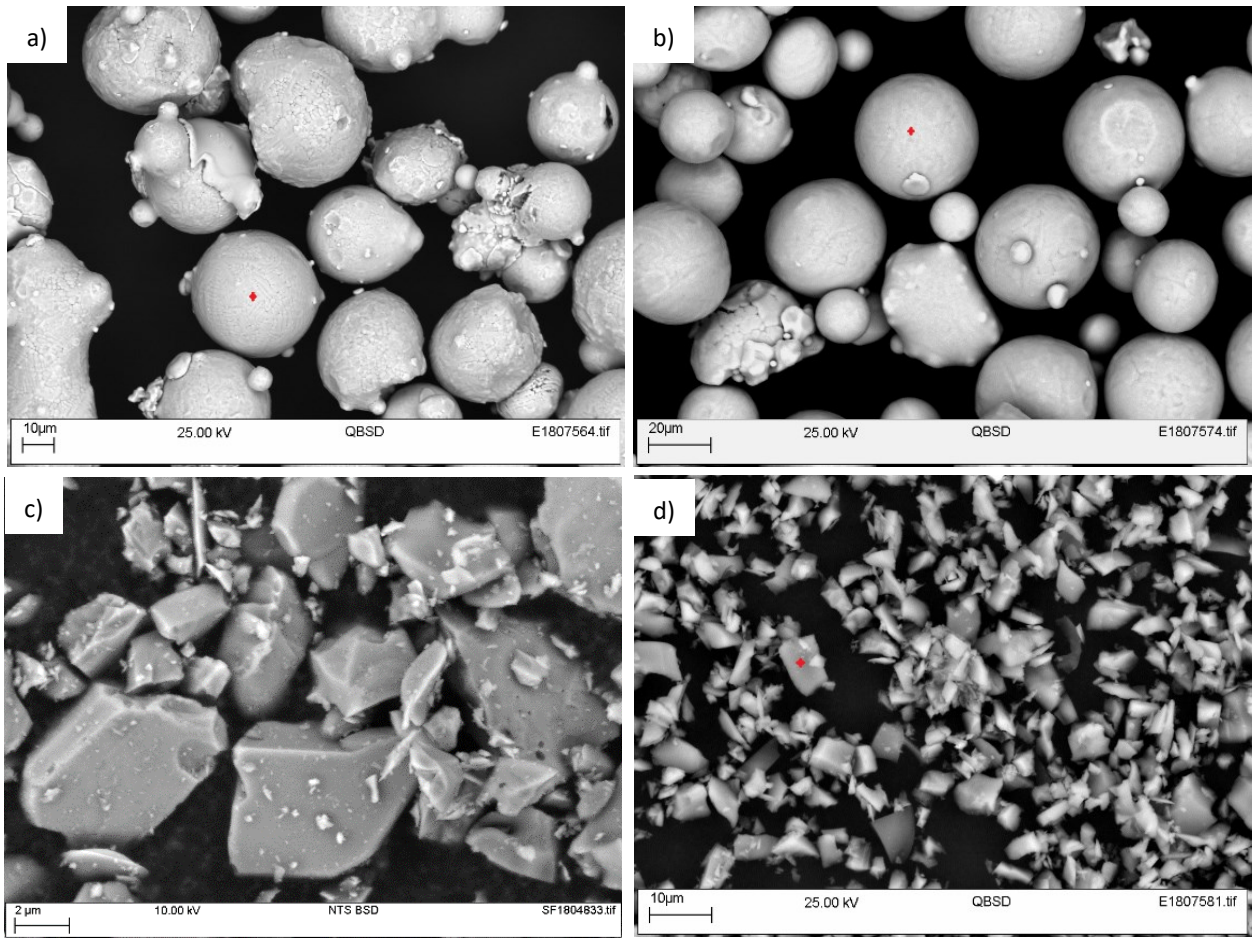

Figure 5 Surface morphology of as-received powders (a) IN625 (b) Ti64 (c) TiB_2 and (d) SiC

BSE images of the cross-sections of IN625 and Ti64 powders are shown in Figure 6a and Figure 6b, respectively. IN625 powder particle shows a cellular microstructure, which is a consequence of the gas atomisation (rapid solidification of the molten alloy) process while the Ti64 powder particle did not reveal any features. BSE images of HIPed IN625 and Ti64 argon gas atomised powders are shown in Figure 7a and Figure 7b, respectively. Both alloys were fully consolidated with no porosity. HIPed IN625 shows a fully recrystallized microstructure, which can be inferred from the presence of annealing twins, highlighted from the grain orientation contrast. The microstructure of HIPed Ti64 was seen to consist of α-Ti and β-Ti phase, with each having different amounts of aluminium and vanadium. Figure 8a and Figure 8b show light optical images of IN625+10%SiC and Ti64+10%TiB_2, respectively. Addition of ceramic phase has resulted in the formation of complex microstructures for both systems. In order to better understand the spatial distribution of various chemical elements, EDX mappings were performed on representative regions.

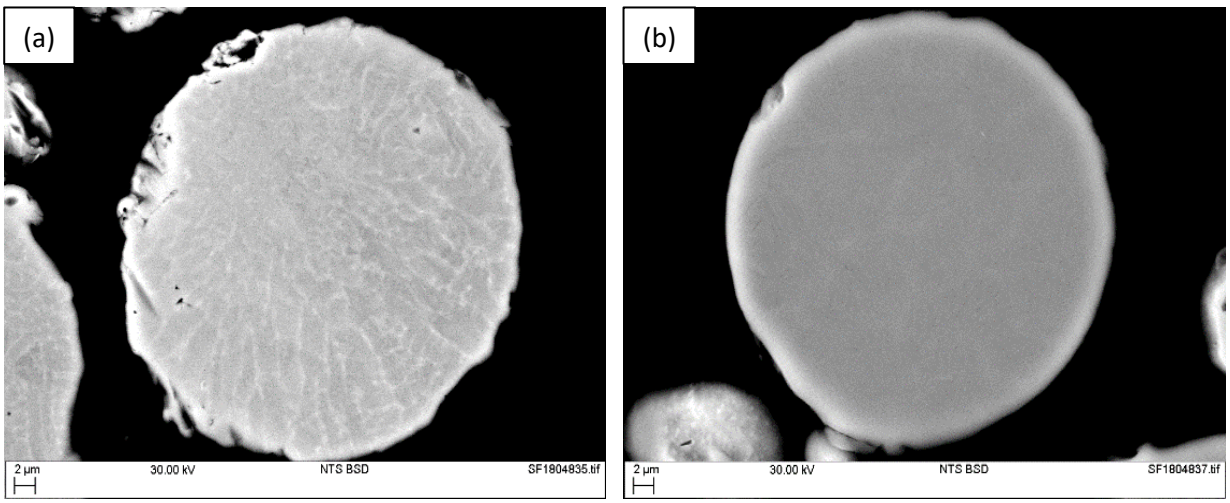

Figure 6 Internal microstructures of the as-received powders (a) IN625 (b) Ti64

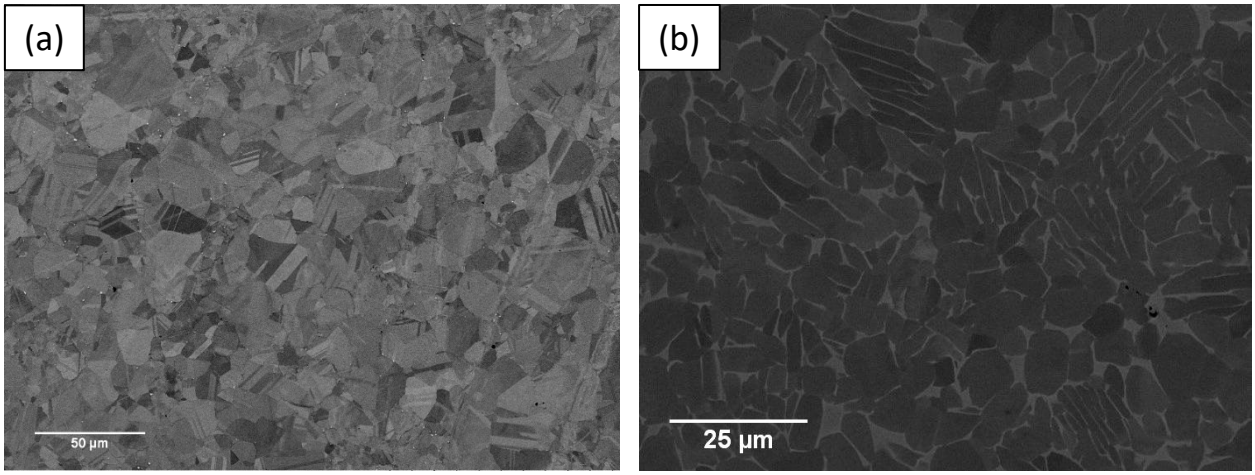

Figure 7 BSE images of (a) HIPed IN625 (b) HIPed Ti64

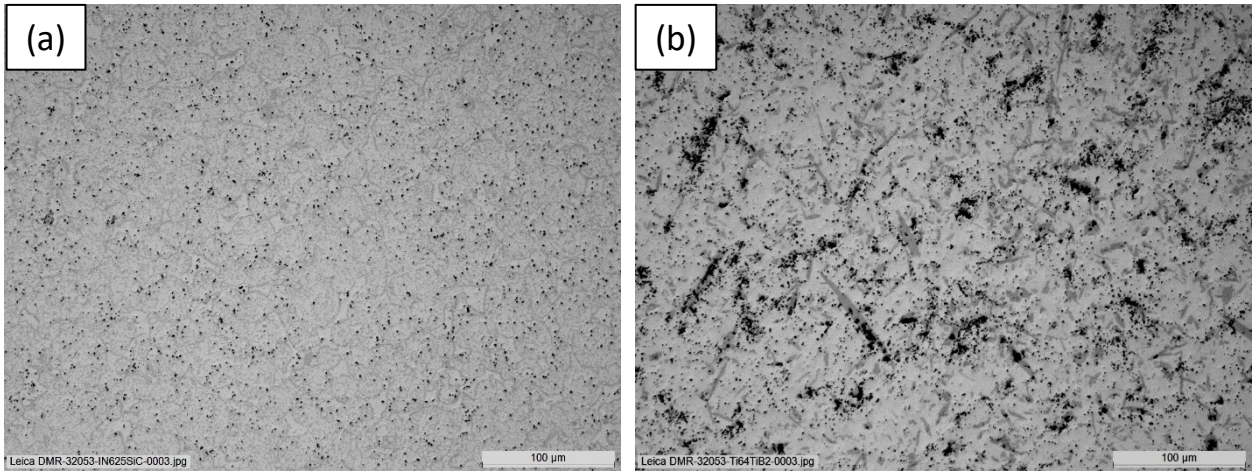

Figure 8 Light optical images of (a) HIPed IN625+10%SiC (b) HIPed Ti64+10%TiB_2

EDX mapping for IN625+10%SiC was performed on regions covering approximately 100µm x 100µm, and are shown in Figure 9. It was evident that the contrast variations observed in the BSE image correlate well with the spatial distribution of the elements. Extensive redistribution of chemical elements occurred during HIPing with regions depleted in nickel and enriched in chromium, niobium, and carbon, suggesting that they are chromium and niobium carbides. The peripheral regions of the AGA IN625 powder were seen to be enriched with molybdenum, silicon, and niobium, while nickel was found to be depleted.

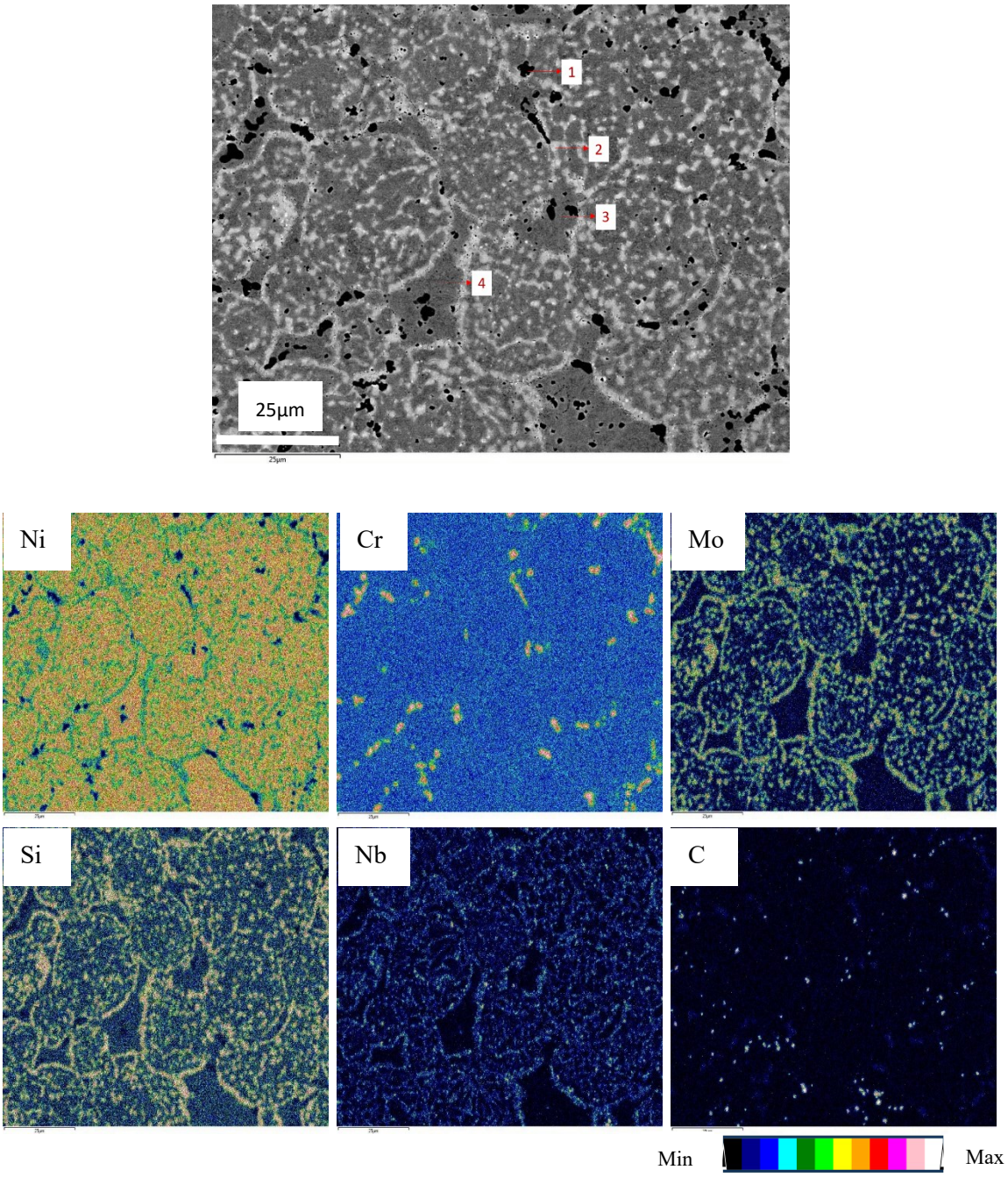

Figure 9 BSE image IN625+10%SiC consolidated via HIP and the corresponding EDS maps of various elements

Semi-quantitative analysis was performed at the points (1 through 4) marked in the BSE image and shown in Figure 10. Carbon was not considered as its analysis is usually found to be unreliable. This has implications on the weight fractions of other elements, and must therefore be used only as a rough guideline.

Quant Results View

Viewed Data: SF/19/178 IN625+10%SiC EDX 1

Processing Option Used: All Elements Processed (Normalized)

Element	Wt%	Wt% Sigma
Si	0.84	0.15
Cr	69.56	0.83
Fe	1.55	0.26
Ni	12.94	0.50
Nb	6.27	0.57
Mo	8.84	0.68
Total	100.00	

Quant Results View

Viewed Data: SF/19/178 IN625+10%SiC EDX 2

Processing Option Used: All Elements Processed (Normalized)

Element	Wt%	Wt% Sigma
Si	6.50	0.27
Cr	21.54	0.55
Fe	1.63	0.28
Ni	37.68	0.81
Nb	4.56	0.73
Mo	28.09	0.93
Total	100.00	

Quant Results View

Viewed Data: SF/19/178 IN625+10%SiC EDX 3

Processing Option Used: All Elements Processed (Normalized)

Element	Wt%	Wt% Sigma
Si	1.36	0.22
Cr	18.64	0.54
Fe	5.12	0.39
Ni	70.41	0.92
Nb	2.31	0.62
Mo	2.17	0.68
Total	100.00	

Quant Results View

Viewed Data: SF/19/178 IN625+10%SiC EDX 4

Processing Option Used: All Elements Processed (Normalized)

Element	Wt%	Wt% Sigma
Si	1.55	0.13
Cr	19.45	0.31
Fe	5.12	0.22
Ni	71.96	0.45
Mo	1.93	0.35
Total	100.00	

Figure 10 Semi-quantitative EDX data at points 1 through 4 marked in the BSE image shown in Figure 9

EDX maps for Ti64+10%TiB_2 are shown in Figure 11. The dark needle shaped precipitates were seen to consist of titanium and boron while the β-Ti regions (with white contrast in the BSE image) are enriched in aluminium and vanadium. Interestingly, the irregular shaped dark precipitates were rich in carbon. Presence of carbon in the specimen was presumably from the mild steel canister material that was used to encapsulate the powder blend for HIPing. Semi-quantitative analysis was performed at the points (1 through 3) marked in the BSE image and shown in Figure 12. The composition for point 3, which is the dark needle shaped precipitate, was consistent with titanium boride (TiB), which forms from the reaction between TiB_2 and Ti ($Ti + TiB_2 \rightarrow 2TiB$).

The Vickers microhardness, erosion-corrosion and room temperature Charpy impact test results are shown in Table 3. Improvement in the hardness values of the IN625 and Ti64 base composites (i.e. IN625+10%SiC and Ti64+10%TiB_2) compared to IN625 and Ti64 can be attributed to the microstructure resulting from the addition of the ceramic phases. Erosion-corrosion data for the specimens suggest that the complex microstructure that forms in IN625 and Ti64 composites due to the addition of ceramic phases improves their erosion-corrosion performance. With the addition of 10%SiC in IN625, the erosion-corrosion rate decreased from 14.08mm/year to 8.35mm/year while addition of 10%TiB_2 to Ti64 has reduced erosion-corrosion rate of Ti64 from 12.85mm/year to 6.8mm/year, showing their positive effect on the microstructure. Compared to the base alloys, room temperature Charpy impact energies of the MMC composites were found to be very low suggesting that they have poor ductility. While the impact energy of HIPed IN625 was 53J, it dropped quite drastically to less than 5J with the addition of ceramic phase. The trend is similar in Ti64+TiB_2 system, although the toughness of Ti64 was lower than that of HIPed IN625 (27J and 53J, respectively). The drop in the toughness clearly shows that the addition of 10vol% of ceramic phase amount of ceramic phase results in the loss of ductility.

Figure 13a and Figure 13b show the BSE images of the surfaces of IN625 and IN625+10%SiC Charpy impact tested specimens, respectively. For both specimens, it appears that the fracture occurred along prior particle boundaries (PPBs) as the fracture surfaces contained spherical features. The oxides/oxycarbides that nucleated along the PPBs during HIPing act as void nucleating sites and de-bond during the fracture. So, essentially, the fracture was still ductile even in IN625+10%SiC, specimen although the energy absorbed was quite low. HIPed Ti64 and Ti64+10%TiB_2 specimens undergo apparent ductile fracture (Figure 14a anc Figure 14b). In Ti64+10%TiB_2, the fracture surface contained traces of needle shapes (Figure 14b), which resembles the morphology of TiB phase, which was embedded in Ti64 (Figure 11a), suggesting that the interface between TiB and the matrix is where the voids nucleate and grow. Figure 15 shows the images of Ti64+10%TiB_2 before and after erosion-corrosion testing. The post-test image also highlights the wear scar caused by the impinging slurry jet – 4mm diameter.

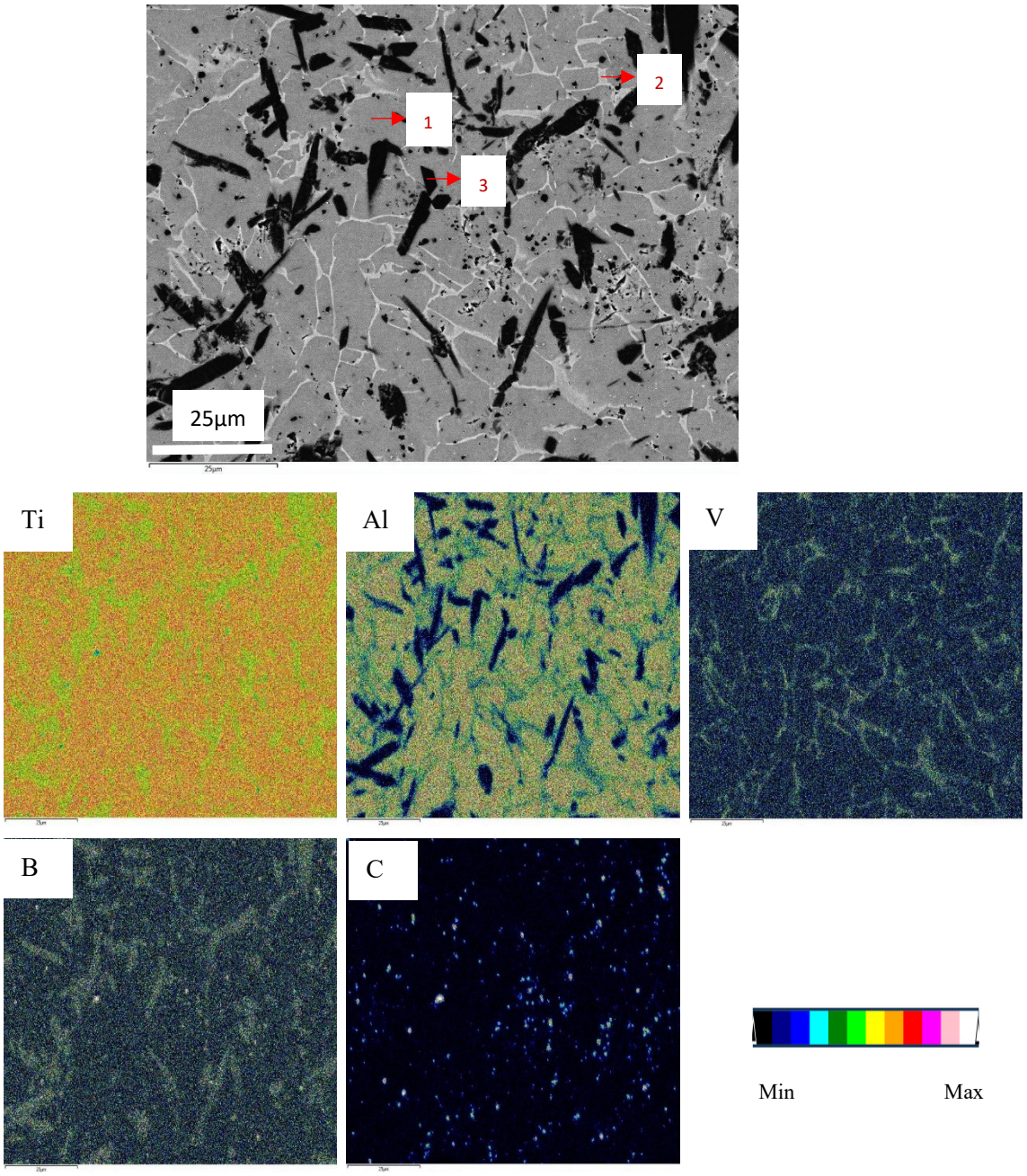

Figure 11 BSE image Ti64+10%TiB_2 consolidated via HIP and the corresponding EDS maps of various elements

Quant Results View

Viewed Data: SF/19/178 Ti64+10TiB2 EDX 1

Processing Option Used: All Elements Processed (Normalized)

Element	Wt%	Wt% Sigma
Al	7.22	0.10
Ti	90.57	0.22
V	2.21	0.21
Total	100.00	

Quant Results View

Viewed Data: SF/19/178 Ti64+10TiB2 EDX 2

Processing Option Used: All Elements Processed (Normalized)

Element	Wt%	Wt% Sigma
Al	3.85	0.23
Ti	81.14	0.73
V	13.55	0.64
Fe	1.47	0.42
Total	100.00	

Quant Results View

Viewed Data: SF/19/178 Ti64+10TiB2 EDX 3

Processing Option Used: All Elements Processed (Normalized)

Element	Wt%	Wt% Sigma
B	16.76	1.10
Al	1.04	0.09
Ti	80.13	1.09
V	2.07	0.31
Total	100.00	

Figure 12 Semi-quantitative EDS data at points 1 through 3 marked in the BSE image shown in Figure 11

Table 3 Vickers microhardness, erosion-corrosion rate, and Charpy impact toughness of IN625, Ti64, IN625+10%SiC, and Ti64+10%TiB_2 specimens

HIP run no.	Composition (Vol%)	Vickers microhardness ($HV_{0.5}$)	Erosion-corrosion rate (mm/year)	Charpy toughness (Joules)
1	IN625	294 ±41	14.08	53
2	IN625+10%SiC	674±108	8.35	2
3	Ti64	328±8	12.85	27
4	Ti64+10%TiB_2	735±102	6.8	2

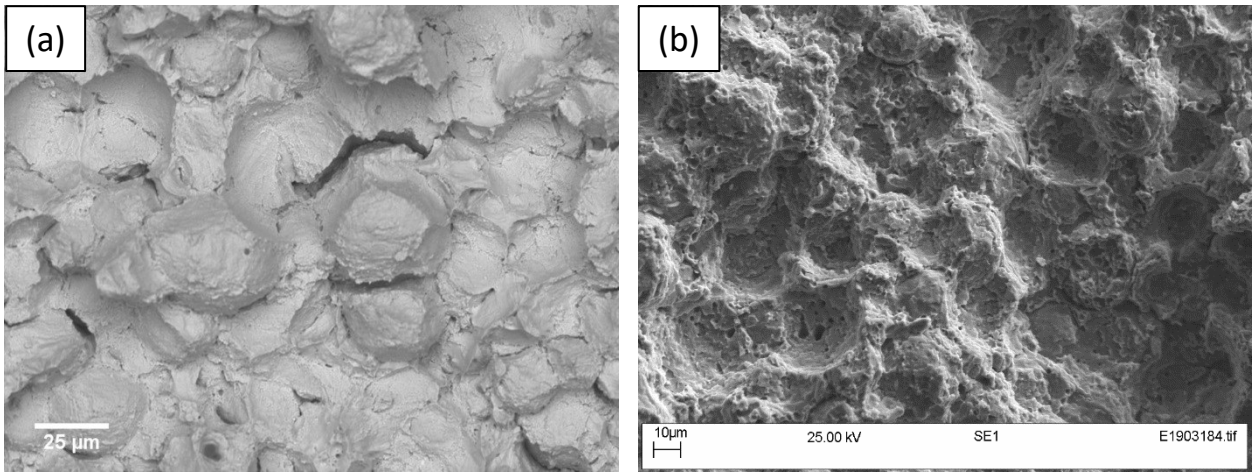

Figure 13 BSE images of the surfaces of the Charpy impact tested specimens (a) IN625 (b) IN625+10%SiC

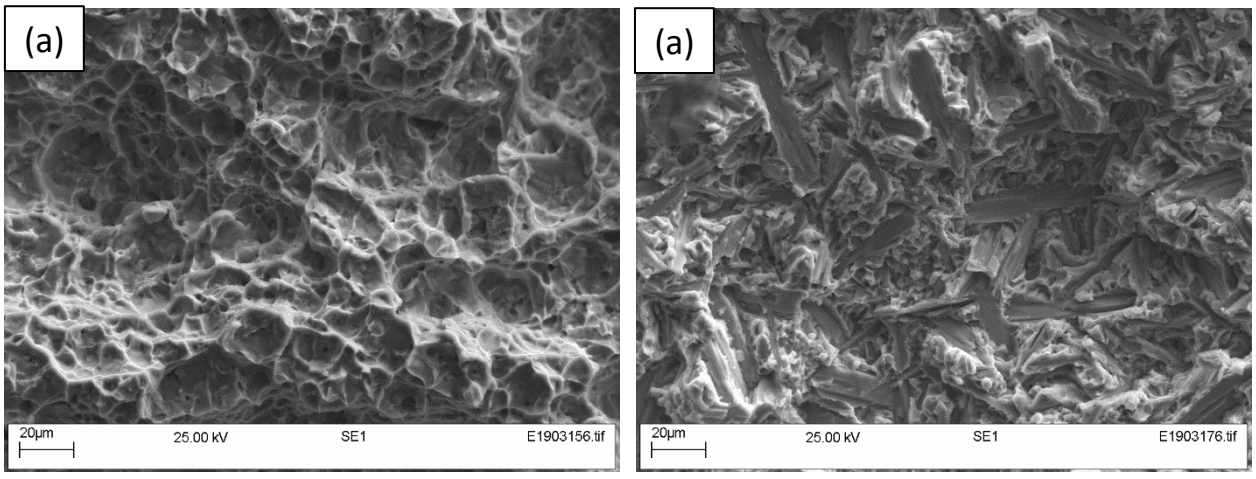

Figure 14 BSE images of the surfaces of the Charpy impact tested specimens (a) Ti64 (b) Ti64+10%TiB2

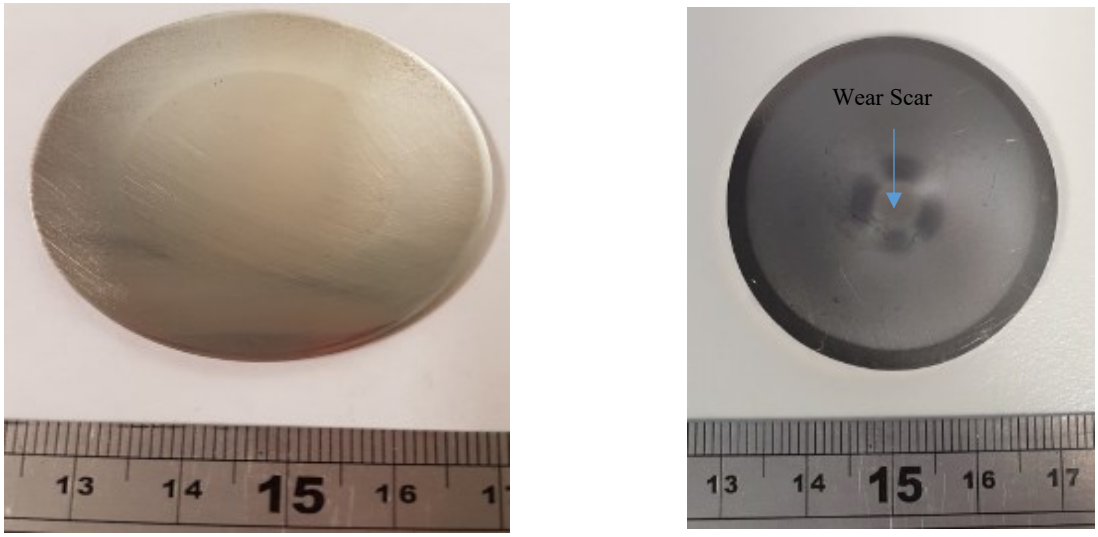

Figure 15: Before and after images of Ti64+10%TiB_2

4 CONCLUSIONS

MMC powders with different volume fractions of the ceramic particles in IN625 and Ti64 powders were produced using Speedmixer™ and consolidated by HIP process. The main findings are summarised as follows:

- IN625 and Ti64 base MMC HIPed materials showed no porosity, although the resulting microstructures were very complex. This was attributed to the application of high isostatic pressures and long dwell times used during HIP consolidation process.
- EDX mapping was performed on the HIP consolidated specimens to obtain the spatial distribution of various elements. Results revealed that an interaction layer between metal and ceramic particles had occurred, with enrichment and a concomitant depletion of certain elements. In addition, precipitates with complex chemistry were also formed.
- Vickers microhardness data of HIPed MMCs clearly showed that, compared to the base alloys (IN625 and Ti64), their hardness has more than doubled. Specifically, with the addition of 10%SiC to IN625, the hardness increased from 294HV 674HV and with the addition of 10%TiB_2 to Ti64, the hardness increased from 328HV to 735HV.
- Erosion-corrosion tests clearly revealed that the microstructures of IN625 and Ti64 base composites formed after HIPing have lower erosion-corrosion rate compared to base alloys, suggesting the positive role of the complex microstructural features formed due to the addition of SiC and TiB_2 to the base powders, respectively.
- Charpy impact tests performed on the HIPed IN625 and Ti64 base MMCs revealed that they possess very low ductility compared to base alloys.
- Addition of 10%SiC in IN625 and 10%TiB_2 in Ti64, respectively, provided materials with higher hardness and lower erosion-corrosion rate compared to the base alloys.

ACKNOWLEDGEMENT

The authors would like to acknowledge the European Commission for funding the H2020 EU project Geo-Coat: Development of novel and cost-effective corrosion resistant coatings for high temperature geothermal applications. Call H2020-LCE-2017-RES-RIA-TwoStage (Project no. 764086) under which the current work was performed.

REFERENCES

S. N. Karlsdottir, "Corrosion, scaling and material selection in geothermal power production," in *Comprehensive renewable energy*, Elsevier, 2012, pp. 241-259.

Kainer, K.U., 2006. Basics of metal matrix composites. Wiley-VCH GmbH & Co. KGaA, Weinheim, Germany.

Atkinson, H. V., and S. Davies. "Fundamental aspects of hot isostatic pressing: an overview." *Metallurgical and Materials Transactions A* 31, no. 12 (2000): 2981-3000.

Wilkinson, D. S., and M. F. Ashby. "Pressure sintering by power law creep." *Acta Metallurgica* 23, no. 11 (1975): 1277-1285.

Helle, A. S., Kenneth E. Easterling, and M. F. Ashby. "Hot-isostatic pressing diagrams: new developments." *Acta Metallurgica* 33, no. 12 (1985): 2163-2174.

Li, E. K. H., and P. D. Funkenbusch. "Hot isostatic pressing (HIP) of powder mixtures and composites: Packing, densification, and microstructural effects." *Metallurgical and Materials Transactions A* 24, no. 6 (1993): 1345-1354.

Kaysser, Wolfgang A., M. Asian, Eduard Arzt, Mirjana Mitkov, and Günther Petzow. "Microstructural development and densification during hipping of ceramics and metals." *Powder metallurgy* 31, no. 1 (1988): 63-69.

Brownlie, F., Anene, C., Hodgkiess, T., Pearson, A., Galloway, A. M. “Comparison of Hot Wire TIG Stellite 6 weld cladding and lost wax cast Stellite 6 under corrosive wear conditions.” *Wear 404-405*, (2018): 71-81